JOURNAL OF SPACECRAFT AND ROCKETS
Vol. 47, No. 6, November–December 2010

Design and Feasibility of ExoMars Supersonic Parachute Scirocco Test

R. Votta,* M. Marini,† F. De Filippis,‡ M. Di Vice,§ and R. Sabatano¶
Centro Italiano Ricerche Aerospaziali, 81043 Capua CE, Italy

DOI: 10.2514/1.50230

A feasibility study of ExoMars parachute supersonic experiment to be possibly performed in the Centro Italiano Ricerche Aerospaziali Plasma Wind-Tunnel Scirocco facility has been analyzed. To verify the test feasibility, some test conditions in terms of facility reservoir conditions have been simulated by means of computational fluid dynamics computations of a modified nozzle, and verified with respect to testing requirements mainly in terms of test article size, Mach number, and dynamic pressure. The proper functioning of the wind tunnel has also been checked. In particular, the facility makes available a 80-MW power vacuum system that guarantees inside the test chamber the low-pressure conditions of the Mars atmosphere into which the parachute is foreseen to be opened. The possibility to introduce an air heater and/or burner would assure also the matching of temperature requirement, and reduce the request of mass flow rate. Computational fluid dynamics simulations of the complete facility configuration (nozzle, test chamber, diffuser) with the test article inside have verified the right functioning of the diffuser (occurrence of tunnel blockage) and the effects of the interaction between the bow shock wave in front of the capsule and the flow exiting from the nozzle, and the pressure that establishes inside the test chamber.

Nomenclature

A, A^*	=	section area, throat section area, m^2
D	=	diameter, m
H	=	total enthalpy per unit mass, MJ/kg
L	=	reference length, m
M	=	Mach number
P	=	total pressure, Pa or bar
p	=	static pressure, Pa or mbar or mm Hg
Q	=	heat flux, kW/m^2
Re	=	Reynolds number
S_{ij}	=	gradients of the main flow velocities
T	=	temperature, K or °R
X, Y, Z	=	frame of reference
Δ	=	variation
η	=	diffuser efficiency
μ	=	viscosity, $kg/m \cdot s$
τ_{ij}	=	stress tensor, N/m^2

Subscripts

0	=	reservoir conditions
L	=	reference length
nsw	=	normal shock wave
S	=	stagnation conditions
vac	=	vacuum system conditions
wall	=	wall

Presented as Paper 2009-7235 at the 16th AIAA/DLR/DGLR International Space Planes and Hypersonic Systems and Technologies Conference, Bremen, Germany, 19–22 October 2009; received 7 April 2010; revision received 1 August 2010; accepted for publication 2 August 2010.

*Ph.D. Research Engineer, Aerospace Propulsion and Reacting Flows Unit; r.votta@cira.it.
†Ph.D. Research Engineer, Aerospace Propulsion and Reacting Flows Unit; m.marini@cira.it.
‡Physicist, Space Systems Unit; f.defilippis@cira.it.
§Research Engineer, Aeronautical Systems Unit; m.divice@cira.it.
¶Research Engineer, Space Systems Unit; r.sabatano@cira.it.

I. Introduction

THE present work concerns with the test feasibility study of the ExoMars parachute scaled model supersonic experiment [1–3], to be possibly performed in the Centro Italiano Ricerche Aerospaziali (CIRA) Plasma Wind-Tunnel Scirocco facility [4,5]. Of course, emphasis is given in the article to the modifications to be realized into the facility to match the test requirements, because Scirocco is usually not devoted to these flow conditions and test logic. The purpose of the activity is the proper characterization of the flow inside the Scirocco facility test-leg to verify both the proper functioning of the wind tunnel and the achievement of customer's testing requirements, particularly in terms of size of test article (composed by a capsule and the parachute), deployment Mach number and dynamic pressure. In particular, the 80-MW power vacuum system fitted to the facility guarantees inside the test chamber the low-pressure conditions of the Mars atmosphere into which the ExoMars parachute is foreseen to be opened.

In the middle of the 1990s the same similar supersonic parachute testing activities were carried out by Martin–Baker Aircraft Company,** in particular for the pilot parachute of the Cassini–Huygens spacecraft, a joint NASA/ESA/ASI mission for the exploration of Saturn, Titan, and the other moons of the Saturn system. More recently, high-altitude subsonic parachute drop tests have been performed [6] for developing and qualifying at Earth a new parachute system for Mars exploration, composed by a subsonic parachute in conjunction with the Viking 16.1 m supersonic parachute as part of a two-stage system. Moreover, lately a series of supersonic wind-tunnel experiments [7] were performed to determine the supersonic performance of a 4% scaled Mars Science Laboratory (MSL) disk-gap-band (DGB) parachute in the wake of a 70-deg sphere-cone entry vehicle with biconic backshell, in support of the MSL parachute development and qualification.

In this work, feasibility and design activities will be carried out by using a state-of-the-art computational fluid dynamics (CFD) code available at CIRA and described in paragraph IV. In particular, a first CFD analysis will be performed to design the nozzle configuration (i.e., the modifications to be applied to the preexisting nozzles) and to define the facility driving conditions able to match as much as possible the customer's testing requirements. The proper functioning of Scirocco subsystems (test chamber, diffuser, vacuum system, etc.)

**Additional data on the ESA Science and Technology: Supersonic Parachute Test available at http://sci.esa.int/science-e/www/object/index.cfm?fobjectid=35017 [accessed May 1995].

in these facility conditions will be also checked. Finally, the analysis will be completed by means of CFD simulations of the complete facility test-leg (nozzle, test chamber, diffuser), with the test article inside, to verify the right functioning of the diffuser, the effects of the interaction between the bow shock in front of the capsule and the flow exiting from the nozzle, the pressure establishing inside the test chamber, and the possible occurrence of cryogenic temperatures harmful to some facility components.

II. Motivations and Study Logic

ExoMars is the first Aurora Flagship mission of the European Space Agency (ESA) to be assessed [1]. Its aim is to further characterise the biological environment on Mars in preparation for robotic missions and then human exploration. Data from the mission will also provide invaluable input for broader studies of exobiology.

This mission calls for the development of a Mars orbiter, a descent module and a Mars rover. The Mars orbiter will have to be capable of reaching Mars and putting itself into orbit around the planet. On board will be a Mars rover within a descent module. After their release and landing on the surface of Mars, the orbiter will transfer itself into a more suitable orbit where it will be able to operate as a data relay satellite. Initially, it will act as a data relay for the ExoMars rover but its life may be extended to serve future missions. The Mars descent module will deliver the rover to a specific location by using an inflatable braking device or a parachute system [1,2]. Both systems are sufficiently robust to survive the stresses of atmospheric entry and their landing accuracy will be sufficient for this mission.

The first stage parachute for the ExoMars probe is an 11-m diameter disk-gap-band (DGB) [2] as depicted in Fig. 1. The maximum deployment Mach number for the mission is 2.1. In the frame of the ESA Huygens program, a DGB parachute of the same configuration was already tested in the AEDC wind tunnel up to Mach 1.5. To extend the available database up to ExoMars maximum Mach number of 2.1 [2,3], a high-speed test of a scaled model of the parachute has been fully defined [3], with the test article being a 7.5% scaled model with a diameter of 0.825 m.

The test has to verify and measure inflation dynamics, inflation stability and drag coefficient at Mach 2.1 in a representative probe wake. Parachute force has to be measured and visual data obtained using high-speed and standard video. This test is the only foreseen verification of the first stage parachute inflation at drag performance at its maximum deployment Mach number. Three different parachutes have to be tested, all of the same design. The characteristics of the test article design [3] are reported in the following Table 1, while a general layout of the parachute scaled model is reported in Fig. 2.

The parachutes are manufactured from low porosity Nylon broadloom fabric with Kevlar lines. The parachute lines are terminated at a metal ring. A Kevlar riser then attaches the confluence ring to a swivel attached to the load cell. The parachutes have to be deployed at a Mach number of between 2.0 and 2.5 and at a dynamic pressure between 2.0 and 5.0 kPa, as reported in the wind-tunnel test definition

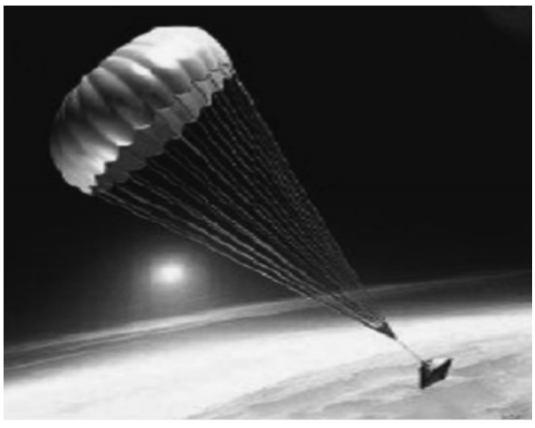

Fig. 1 ExoMars first stage parachute.

Table 1 Test article characteristics [3]

Reference diameter	0.825 m
Flying diameter	0.594 m
Reference area	0.535 m^2
Maximum Drag Coefficient	0.48
Geometric Porosity	22.4%
Line length	1.65 m
Flying length (confluence to vent)	1.92 m
Number of lines	20
x/D (trailing distance/forebody diameter measured from base of forebody to parachute mouth)	10.0
Mass	0.2 kg

[3]. A support strut shall be installed which provides a hard-point on the tunnel centerline. A load cell and a swivel are mounted on the downstream side of the strut. A clevis is attached to the load cell to enable attachment of the test parachute. The strut is streamlined to reduce the wake effects on the parachute, while a forebody representative of the ExoMars entry module (i.e., a capsule) is attached to the strut in front of the load cell. The forebody entry capsule model has a diameter of 0.255 m. Before deployment, the parachute is packed in a deployment can directly behind the ExoMars entry module model. On command, the parachute is ejected into the air stream. The parachute bag detaches from the parachute at lines-taut and is caught in the tunnel cooler downstream of the test section.

As far as ExoMars mission analysis and design are concerned [8], the testing requirements for the test article (composed by the capsule and the parachute) in scale 7.5% of the full vehicle, reproducing Mars atmosphere, are the following: 1) CO_2 atmosphere, 2) $M = 2.1$, 3) $P_{\text{dyn}} = 910$ Pa, and 4) $T = 231$ K.

The present work relies on the test feasibility on CIRA Scirocco Plasma Wind Tunnel and the modifications to be applied to the facility to match the above test requirements, because Scirocco is not devoted to these flow conditions and test logic. It is worth it to underline that the large Scirocco test chamber guarantees the test article size with at least 3.4 m available length, and the 80-MW power vacuum system guarantees the extremely low-pressure conditions ($P_{\text{dyn}} < 1$ kPa) of the Mars atmosphere into which the parachute is foreseen to be opened, as it will be shown in the following sections.

Figure 3 shows the performed study logic. First of all, a preliminary CFD analysis has been performed to evaluate the nozzle configuration (i.e., the modifications to be applied to the preexisting nozzles) and the requirements verification. The output of this first analysis is the definition of the test. This analysis will be presented in the Sec. V, after a description of the Scirocco Plasma Wind Tunnel presented in Sec. III, and will be followed by Sec. VI, where the proper functioning of Scirocco subsystems (test chamber, diffuser, vacuum system, etc.) in these facility driving conditions has also been checked. Finally, the second part of test feasibility analysis has been devoted to CFD simulations of the complete facility configuration (nozzle, test chamber, diffuser) with the test article inside. This analysis will be presented in the Sec. VII.

III. Scirocco Plasma Wind Tunnel

The CIRA Plasma Wind Tunnel (PWT) Scirocco [4,5] is devoted to aerothermodynamic tests on full-scale components of aerospace vehicles, and its primary mission is to simulate the thermo-fluid-dynamic conditions suffered by the Thermal Protection System

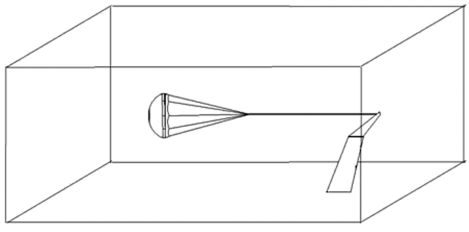

Fig. 2 General layout of test article.

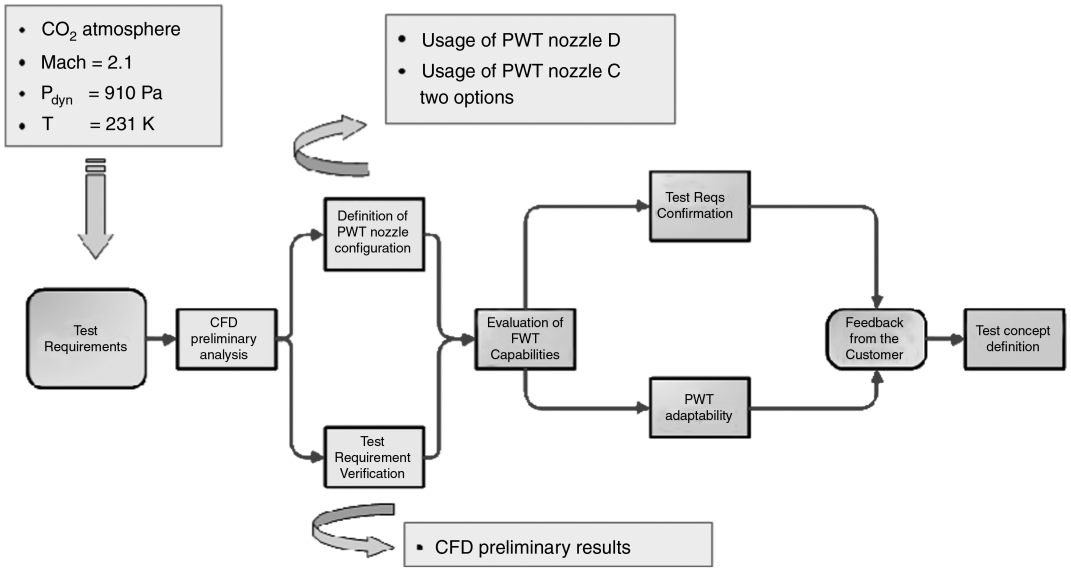

Fig. 3 Study logic.

(TPS) of space vehicles reentering the Earth atmosphere. Scirocco is a very large size facility (see Fig. 4) whose hypersonic jet impacts the test article having a diameter size up to 2 m and reaches Mach number values up to 11. The large test chamber is a cylinder 9.2 m high and with a 5-m diameter. The jet is then collected by a 50-m long diffuser and cooled by an heat exchanger. 70 MW electrical power is used to heat the compressed air that expands along a convergent-divergent conical nozzle. Four different nozzle exit diameters are available: 0.9, 1.15, 1.35 and 1.95 m, respectively, named C, D, E and F. The overall performance of Scirocco in terms of reservoir conditions is the following: total pressure (P_0) varies from 1 to 17 bar and total enthalpy (H_0) varies from 2.5 to 45 MJ/kg. Facility theoretical performance map in terms of reservoir conditions produced by the arc heater is shown in Fig. 5. Lower enthalpy values are obtained by using a mixing plenum chamber between the arc heater column exit and the nozzle inlet convergent part, which allows transverse injection of high-pressure ambient air to reduce the flow total enthalpy.

The energetic heart of the facility is the segmented constricted arc heater, a column with a maximum length of 5.5 m and a bore diameter of 0.11 m. At the extremities of this column there are the cathode and the anode between which the electrical arc is generated. A power supply feeds the electrical DC power to the electrodes for the discharge. A compressed air supply distributes dry compressed air to the various segments of the arc heater column, being able to supply a mass flow rate ranging from 0.1 to 3.5 kg/s, heated up to 10,000 K. One of the most important subsystems of the facility is the vacuum system which generates the vacuum conditions in test chamber required by each test. The system consists of ejectors that make use of high-pressure water steam as motor fluid (30 bar and 250 °C), with a maximum of 80 MW required power.

The achievement of the desired operating conditions in test chamber is assured by the presence, before the insertion of the model by means of a robotized-type support system, of a 100 mm-diameter hemispherical calibration probe made of copper, actively cooled, that measures radial profiles of stagnation pressure (P_S) and stagnation heat flux (Q_S) at a section 0.375 m downstream of the conical nozzle exit section, by means of high precision pressure transducers and Gardon–Gage heat flux sensors, respectively. Facility regulations (mass flow, current) are tuned to measure on the calibration probe the prescribed set point in terms of the couple (P_S, Q_S) which corresponds to the desired couple (P_0, H_0) [5].

Beyond the calibration probe and pressure transducers to monitor the test leg, the facility is equipped by extensive instrumentation, in particular: infrared thermocameras with focusing optics and special filters, spectral range of $8 \div 12$ μm, temperature range up to 2500 °C, installed at the test chamber windows; dual-color and single-color pyrometers for spot measurements for temperature range up to 3000 °C; electronics for the acquisition of pressure channels and thermocouples channels for test articles; emission spectroscopy laser system for the measurements of plasma flow temperatures and species concentrations. Furthermore, two high-resolution video-cameras are installed at the test chamber windows for model and flow visualization during the test run.

The Plasma Wind Tunnel Scirocco has been recently involved in test campaigns related either to components of the ESA ballistic reentry capsule EXPERT either to those of the future CIRA winged reentry vehicle USV_X, and a well assessed test design methodology

Fig. 4 Aerial view of the PWT facility.

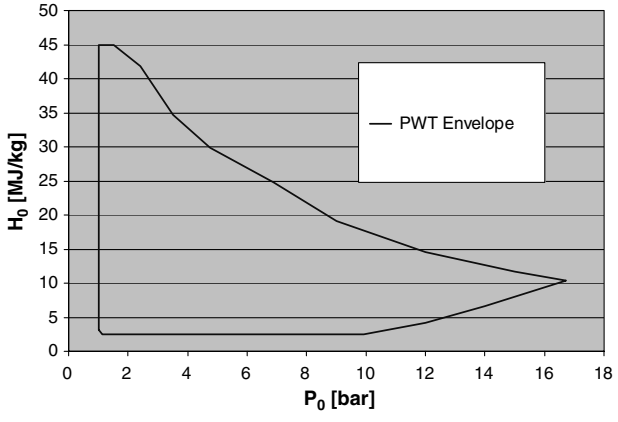

Fig. 5 Arc heater theoretical performance map.

[9] for these flight-relevant experiments has been set up to match test requirements on test articles.

IV. CFD Code

The H3NS CFD code solves the full Reynolds-averaged Navier–Stokes (RANS) equations and considers the air flow in thermochemical nonequilibrium because the code is mainly devoted to simulate hypersonic flowfields.

The modelization of these phenomena is quite difficult because of the difference among the characteristic times of fluid-dynamics and the one of chemical reactions and vibration. This situation generally leads to the thermochemical nonequilibrium. In fact, there are many problems in high-speed gas dynamics where the gas does not reach the equilibrium state: a typical example is the flow across a shock wave, where the pressure and temperature rapidly increase through the shock front. By the time equilibrium properties have been approached, the fluid element has moved a certain distance downstream the shock front. Hence, there is a nonequilibrium region behind the shock wave. As a consequence, the modelization of these phenomena cannot be limited to a calculation of equilibrium conditions at a certain temperature, but a number of equations must be added to the classical Navier–Stokes formulation, one for each dissociating and/or vibrating species. Nevertheless, the code is also able to solve Navier–Stokes equations for ideal gas behavior.

For what concerns the physical modelling, Park's model with five species (O, N, NO, O_2, N_2) and 17 chemical reactions [10] is implemented and the energy exchange between vibrational and translational temperature is based on Landau–Teller nonequilibrium equation, with average relaxation times taken from the Millikan-White [11] theory modified by Park [12]. The viscosity coefficient for the single specie is computed by means of Yun and Mason collision integrals [13], while the conductivity coefficient using Eucken's law. These coefficients for the gas mixture are calculated using semiempirical Wilke's formulas. Diffusion coefficients are obtained by Yun and Mason tabulated collision integrals [13].

Turbulence effects are modeled both with the original Myong–Kasagi [14] two-equation k-ε model and the compressible version proposed by Grasso and Falconi [15]. These models are based on the concept of the eddy viscosity (μ_t) which relates the Reynolds stresses (τ_{ij}^t) to the gradients of the main flow velocities (Sij).

From the numerical point of view, the code is based on a finite volume approach with a cell centered formulation. The inviscid fluxes are computed by using a Flux Difference Splitting scheme [16], where second order approximation is obtained with an Essentially Not Oscillatory (ENO) reconstruction of interface values. Time evolution is performed by an explicit multistage Runge-Kutta algorithm coupled with an implicit evaluation of the source terms.

V. Definition of Plasma Wind Tunnel Nozzle Configuration

To match the ExoMars supersonic parachute test requirements two wind-tunnel existing nozzle configurations have been considered: nozzle D (1.15 m exit diameter) and nozzle C (0.9 m exit diameter).

Figure 6 shows a sketch of the preexisting conical nozzle D half geometry devoted to hypersonic flow conditions (characterized by an area ratio $A/A^* = 2.96$), to be modified to match test requirements, while Fig. 7 reports the concept design of the nozzle D. At the beginning, two technical solutions were identified to achieve $M = 2.1$ ($A/A^* = 1.80$) inside the test chamber with using nozzle D: 1) a conical internal thickening to reduce the area ratio A/A^*, or 2) to cut it in length to obtain the proper value of area ratio.

In any case, a new convergent portion of the nozzle has been designed (1 m inlet diameter, 0.5 m length) that interfaces smoothly (i.e., a continuum curve with his derivative) to the inlet section of the conical nozzle, and it assures the achievement of sonic conditions at the throat (i.e., the inlet of the conical nozzle sector). Figure 8 shows the geometrical representation of the conical nozzle D together with the new convergent portion, while Figs. 9 and 10 illustrate the concept designs.

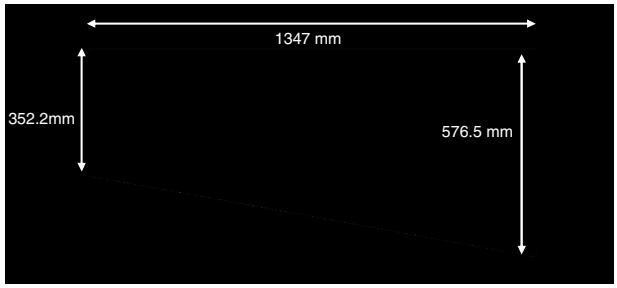

Fig. 6 Nozzle D geometric dimensions.

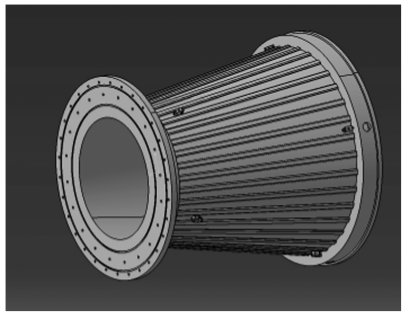

Fig. 7 Nozzle D.

All the mechanical interfaces with the facility components (arc heater column from one side and test chamber from the other side) have been properly checked, of course, and feasible solutions for manufacturing and interfacing the additional parts have been developed.

Some test conditions in terms of reservoir pressure and reservoir temperature (or total enthalpy) and mass flow rate have been simulated and verified with respect to testing requirements by means of CIRA CFD code H3NS. The first analysis has been conducted on nozzle D existing configuration (see Fig. 8).

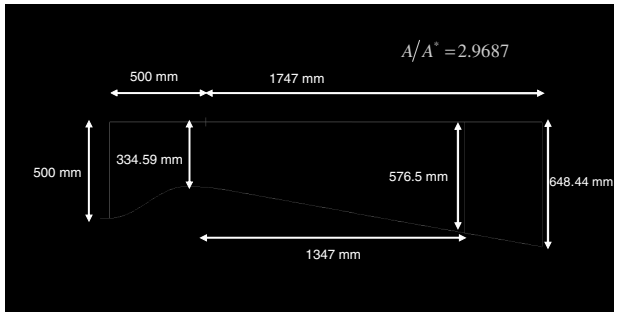

Fig. 8 Modified nozzle D.

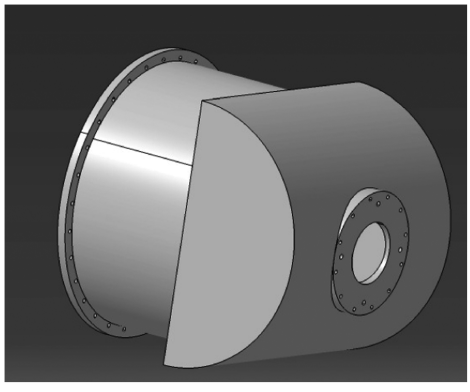

Fig. 9 New convergent portion.

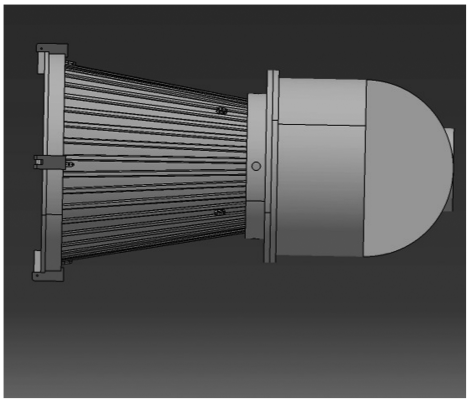

Fig. 10 Nozzle D and convergent.

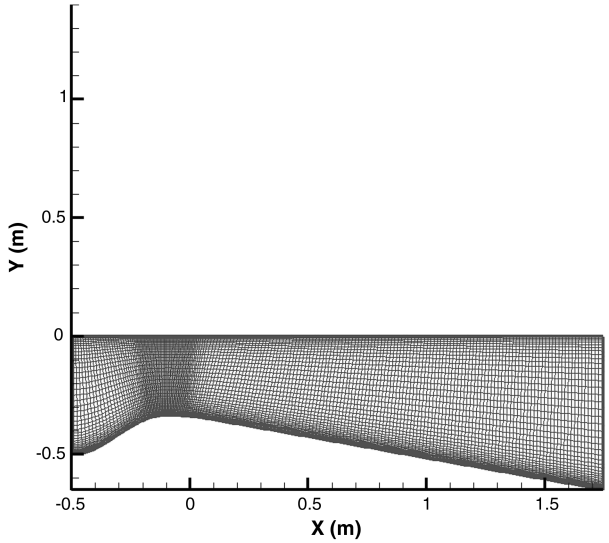

Fig. 11 Nozzle D computational grid.

In the present CFD simulations the flow has been considered axisymmetric in the hypothesis of ideal gas behavior, fully laminar or fully turbulent (k-ε eddy viscosity modelling by Myong and Kasagi [14]), and the wall has been modeled as a cold wall ($T_{\text{wall}} = 300$ K). The selected turbulent model is good enough to describe the typical turbulent boundary layer behavior with respect to the laminar case.

In particular, Table 2 reports the selected conditions for CFD simulations. These conditions are the output of a feasibility study that has considered the facility performance map, the testing requirements (in particular, the low dynamic pressure of a typical Mars entry) and the theoretical-empirical laws that properly describe the functioning of the Scirocco Plasma Wind-Tunnel facility [5].

The computational grids for the numerical flow simulations reported in this paper have been generated by means of the commercial software package ANSYS ICEMCFD®. Grids, composed by quadrilateral elements, have been generated for the symmetry plane (i.e., in the axisymmetric hypothesis) by using a multiblock approach, and have been stretched normally to the solid surfaces to properly predict the different boundary layers developing around the geometric configuration and the localized peak values of thermomechanical loads; moreover, grid points have been clustered in presence of corners, edges and rounded details. The grid topologies have been created in such a way to accurately define all the geometric details of the configurations, i.e., using the necessary number of O-grids. In addition, when necessary grid adaptation to bow shock wave surfaces has been performed. Moreover, a stretching of the grid by using a first cell size equal to 10^{-6} m has been used to reach an Y^+ (nondimensional wall distance) less than one. Figure 11 shows the used monoblock computational grid for nozzle D configuration, composed by 15,840 points and 15,563 cells, where the clustering of points at nozzle throat, to better predict the sonic line, and the cell stretching at nozzle surface can be appreciated. The choice of this kind of grid is the simplicity of the topology. The grid is composed by three grid levels, and no differences have been found between the second and the third level in terms of the most sensitive variables (i.e., heat flux and skin friction), so the grid independence has been demonstrated. The present results rely on the finest grid level.

First of all, it must be said that the requested use of CO_2 as working gas appears too expensive in terms of facility modifications, so the use of air is suggested to contain the cost of the test campaign. Then, the following analysis has been conducted by using air.

In Fig. 12 the achievement of the sonic condition (i.e., of the critical pressure and mass flow rate) into the throat has been verified for all the cases reported in Table 2, while Fig. 13 shows the Mach number contour map for the case EXM-1 of Table 2 as an example of the predicted expansion flow inside the nozzle.

Figures 14–17 report, respectively, the pressure, dynamic pressure, Mach number, and static temperature profiles at the nozzle D exit section for the performed computations EXM-1 and EXM-3 of Table 2 compared with the test requirements.

Table 3 reports for the entire test matrix the predicted nozzle exit conditions (at centerline) and 10 cm forward that is assumed as the position of the capsule stagnation point inside the test chamber. As expected, exit Mach number value is driven only by the area ratio $A/A^* = 2.9687$, thus resulting nearly 25% larger than the requirement. Moreover, no significant effect of laminar or turbulent boundary layer assumption inside the nozzle (see EXM-1 and EXM-2 cases) has been recognized, while a strong effect of T_0 (550 K instead of the ambient 300 K) has been predicted for better matching temperature and reducing mass flow rate (by comparing cases EXM-3 and EXM-1, see Fig. 17). This means that an air heater and/or burner would be necessary to match temperature testing requirement and reduce the necessary mass flow rate. Furthermore, a strong effect of reservoir pressure P_0 is observed in reducing mass flow rate and Reynolds number, as expected by theory.

Finally, Table 4 compares the ExoMars supersonic parachute test requirements and the obtained results.

To improve the performance of the upgraded Scirocco facility with respect to test requirements, and considering the theoretical value of the area ratio ($A/A^* = 1.80$) necessary to achieve $M = 2.1$ in test chamber, existing nozzle C configuration has been considered instead of modifying nozzle D as said previously (through internal thickening or nozzle length shortening). Nozzle C is characterized by the same semicone angle of nozzle D, but it is shorter thus the area ratio is just the desired value $A/A^* = 1.80$.

Nozzle C configuration (see Fig. 18) has been then simulated for best efficiency condition EXM-4 of Table 2, that is a compromise between the driving parameters of the ExoMars supersonic parachute test, i.e., the Mach number and the dynamic pressure. Predicted flowfield in terms of Mach number contours is shown in Fig. 19.

Table 2 Nozzle D test matrix

#	P_0, Pa	T_0, K	H_0, MJ/kg	Re_L	Mass flow rate, kg/s	Flow
EXM-1	4000	300	0.3026	3.0891E + 05	3.65	laminar
EXM-2	4000	300	0.3026	3.0891E + 05	3.65	turbulent
EXM-3	4000	550	0.5547	1.4879E + 05	2.71	laminar
EXM-4	3000	300	0.3026	2.3168E + 05	2.74	laminar
EXM-5	2000	300	0.3026	1.5445E + 05	1.83	laminar

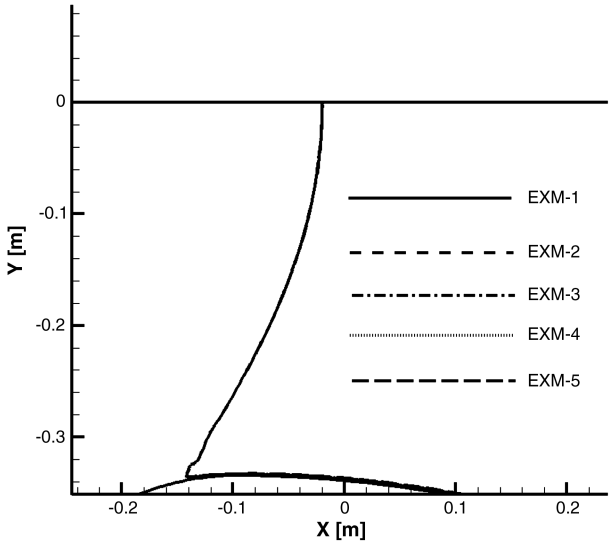

Fig. 12 Nozzle D sonic lines.

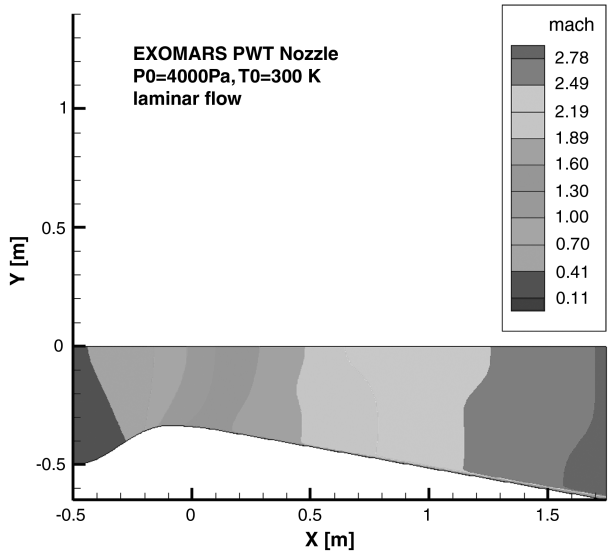

Fig. 13 Nozzle D Mach number contour map.

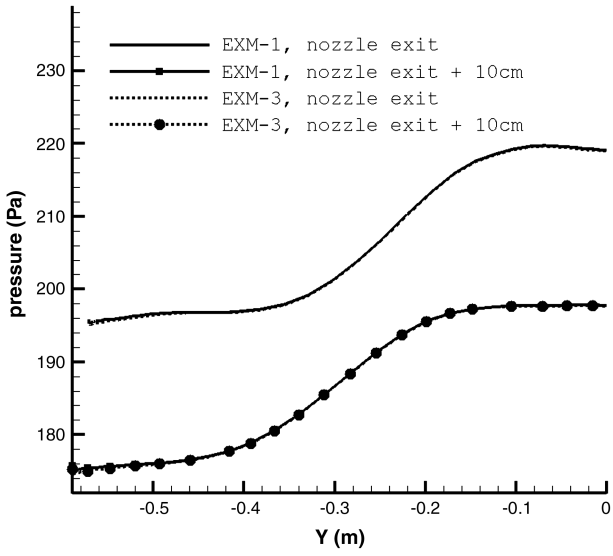

Fig. 14 Nozzle D configuration: pressure exit profiles.

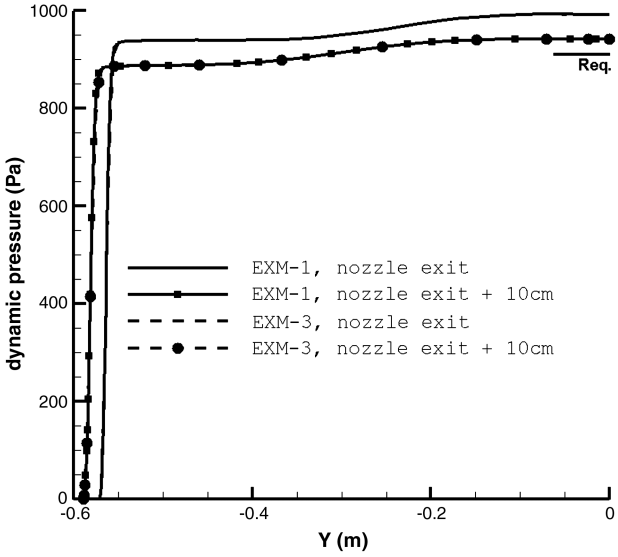

Fig. 15 Nozzle D configuration: dynamic pressure exit profiles.

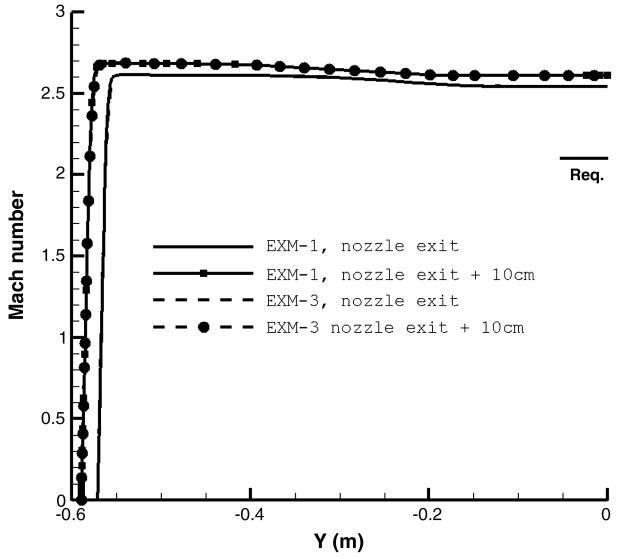

Fig. 16 Nozzle D configuration: Mach number exit profiles.

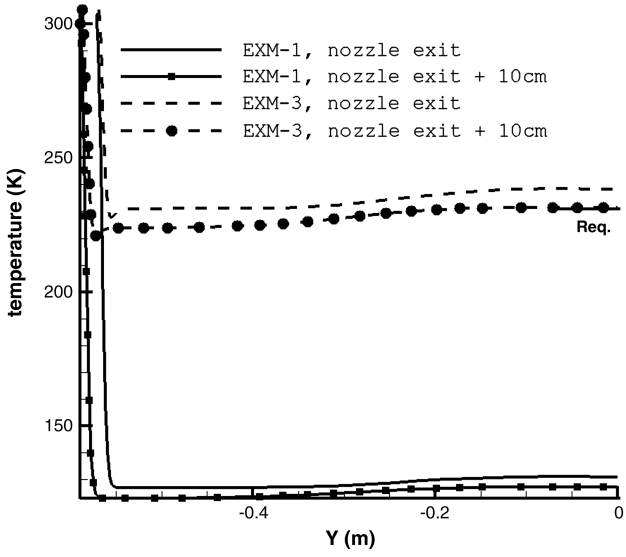

Fig. 17 Nozzle D configuration: temperature exit profiles.

Table 3 Nozzle D predicted exit conditions

	Nozzle exit section				Nozzle exit section + 10 cm			
#	M	P, Pa	T, K	P_{dyn}, Pa	M	P, Pa	T, K	P_{dyn}, Pa
EXM-1	2.6096	197.140	126.9550	941.1040	2.6673	177.8400	123.2230	892.3170
EXM-2	2.6004	200.2500	127.4810	947.8670	2.6662	180.8880	123.8300	900.1260
EXM-3	2.6099	197.3120	231.2850	940.8320	2.6675	177.7850	224.5010	892.1500
EXM-4	2.5457	163.4800	130.5990	741.6070	2.6134	147.1990	126.7430	703.7440
EXM-5	2.5411	109.7740	130.8680	496.1630	2.6081	99.9452	127.0420	471.1190

Table 4 Nozzle D summary of results

Testing requirements	CFD results (nozzle D exit)
CO_2 atmosphere	Air, ideal gas
Mach = 2.1	Mach = 2.54–2.60
P_{dyn} = 910 Pa	P_{dyn} = 500–940 Pa
T = 231 K	T = 126–231 K

The analysis of Figs. 20–22, where respectively Mach number, dynamic pressure and static temperature profiles at nozzle C exit section are reported, shows a much better matching with ExoMars supersonic parachute test requirements. In particular, the analysis of Fig. 22 suggests once more that, for the nozzle C too, the use of an air heater and/or burner to better match temperature requirement is recommended and, as a consequence, also the necessary mass flow rate would be reduced.

Table 5 summarizes the results obtained by simulating nozzle C configuration and condition EXM-4, and the good matching with ExoMars supersonic parachute testing requirements can be appreciated.

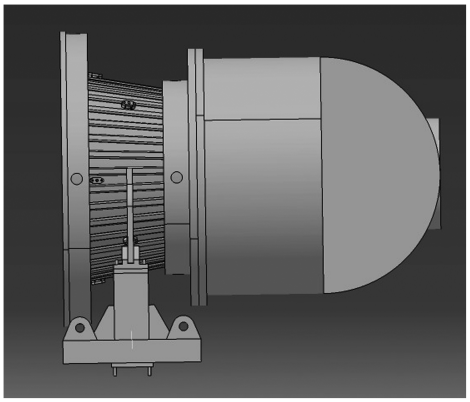

Fig. 18 Nozzle C and convergent.

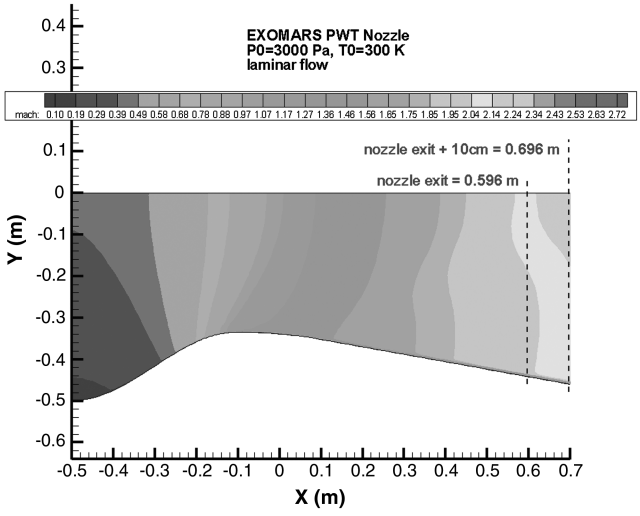

Fig. 19 Nozzle C Mach number contour map.

VI. Verification of Air Liquefaction, Facility Needs, and Diffuser Efficiency

In this section the proper functioning of the Plasma Wind-Tunnel facility has been checked in the selected test conditions (from Table 2), either in terms of air liquefaction inside the test chamber, either in terms of requirements for the subsystems such as the vacuum system and the supersonic diffuser.

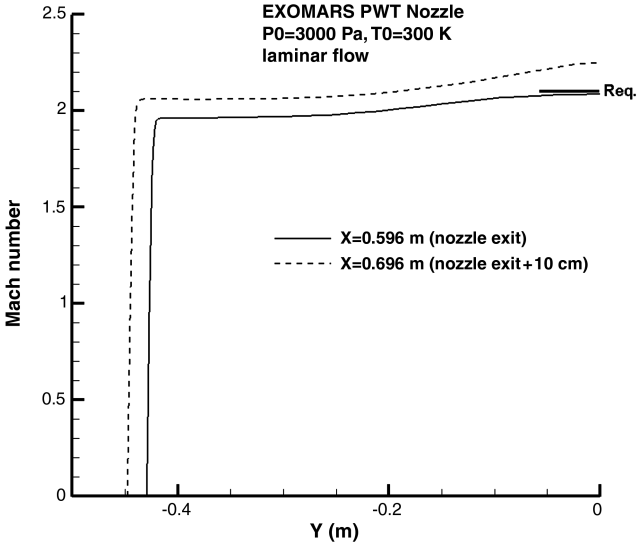

Fig. 20 Nozzle C configuration: Mach number exit profiles.

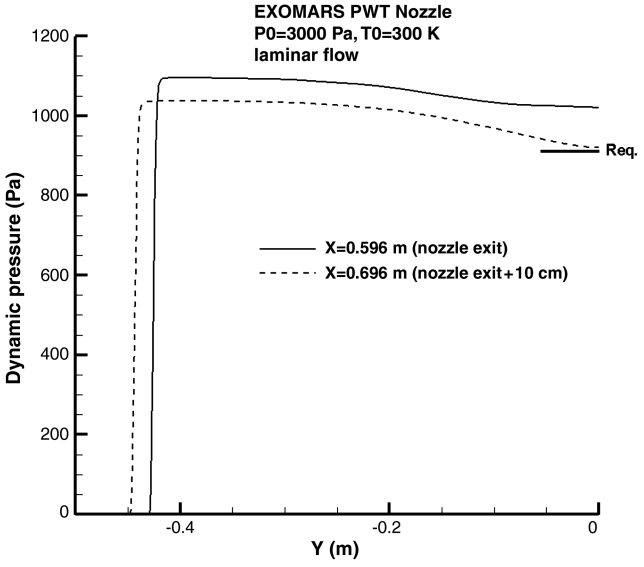

Fig. 21 Nozzle C configuration: dynamic pressure exit profiles.

As far as air liquefaction inside test chamber is concerned, it is well known that this is a typical problem of supersonic wind tunnels [17].

One of the common procedures to solving the problem of condensation [17] in supersonic tunnels is to dry the air, and this is usually done in Scirocco facility because the arc heater is already fed by dry compressed air. Figure 23 verification of air liquefaction in selected ExoMars-PWT conditions shows the predicted test chamber conditions (in terms of static pressure in [mmHg] and static temperature in [°R]) for the selected test conditions of Table 2, compared with experimental data of wind-tunnel nozzles at beginning of liquefaction [17], i.e., air liquefaction occurs above the solid line. As clearly observed, there are large safety margins concerning the occurrence of air liquefaction inside the test chamber, being the test chamber temperatures predicted for nozzle D (Table 3) more than 100°R greater than static saturation temperatures at those pressures (the dashed line). Much better condition is the one predicted for nozzle C (Table 5), where static temperature inside the test chamber is nearly 50°R greater than those of nozzle D conditions.

Regarding the requirements which are reversed to facility subsystems for realizing the selected test conditions of Table 2, the necessary mass flow rate and test chamber pressure to be realized by the vacuum system are reported as diamonds in function of the reservoir pressure P_0 respectively in Figs. 24 and 25. The identified variations of these quantities, i.e., mass flow rate ranging from 1.83 to 3.65 kg/s and test chamber static pressure ranging roughly from 1 to 2 mbar, are compliant with the Plasma Wind Tunnel current capabilities. It must be remarked the fact that, as also shown in Fig. 24, the presence of an air heater and/or a burner (i.e., $T_0 = 550$ K instead of $T_0 = 300$ K) could allow for not only a better matching of temperature test requirement, but also for a considerable reduction of the necessary mass flow rate at the same test chamber pressure.

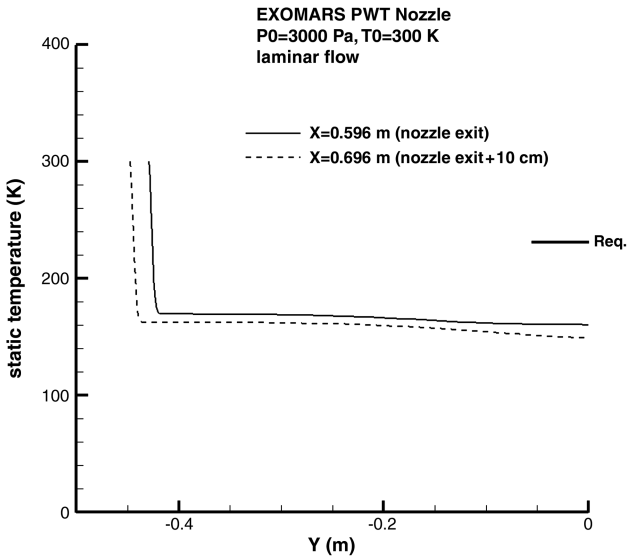

Fig. 22 Nozzle C configuration: temperature exit profiles.

Table 5 Nozzle C Summary of results

Testing requirements	CFD results (nozzle C exit)
CO_2 atmosphere	Air, ideal gas
Mach = 2.1	Mach = 2.0988
$P_{dyn} = 910$ Pa	$P_{dyn} = 1013.22$ Pa
$T = 231$ K	$T = 159.43$ K

Regarding the supersonic diffuser efficiency Fig. 26 reports the predicted Plasma Wind-Tunnel Scirocco diffuser efficiency (labeled ... in the figure) in function of the nozzle exit Reynolds number, compared with measured efficiencies from different models and sources [17–19]. It can be observed that, as Reynolds number is greater than 10^5, the Scirocco diffuser efficiency lays between 0.8 and 1. Note that the diffuser efficiency η can be defined as [20]:

$$\eta = \frac{\Delta p_{\text{actual}}}{\Delta p_{\text{nsw}}} \tag{1}$$

where $\Delta p_{\text{actual}} = p_{\text{vac}}/p_{\text{exit}}$ is the ratio of vacuum system pressure to test chamber pressure (i.e., nozzle exit), and Δp_{nsw} is the pressure rise across an ideal normal shock wave that occurs inside the diffuser at the test chamber Mach number (the hypothesis is to consider a free stream not disturbed by the model). Entering in the Scirocco vacuum system performance map [21] of Fig. 27, and considering the selected driving conditions (Table 2) and the predicted test chamber conditions (Table 3 and 5), the diffuser efficiencies can be then preliminarily estimated through Eq. (1).

Table 6 reports the predicted values of Scirocco diffuser efficiency in the selected ExoMars-PWT conditions. Efficiency η ranges roughly between 0.75 and 1 for Reynolds number greater than 10^5, thus confirming the proper functioning of this critical subsystem, i.e., that the diffuser recovery pressure is close to the normal shock wave one.

VII. Test Simulations

Once the facility conditions able to match test requirements have been selected (EXM-4: $P_0 = 0.03$ bar, $T_0 = 300$ K, mass flow rate = 2.74 kg/s, working gas air, no risk of liquefaction), the second part of test feasibility analysis has been devoted to CFD simulations of the complete facility configuration (nozzle, test chamber, diffuser) with the test article inside. Figure 28 shows a sketch of the complete test configuration, where only the diffuser entry is shown for clarity. In this figure, the positioning of the capsule and the parachute (modeled as a flat plate in absence of information,

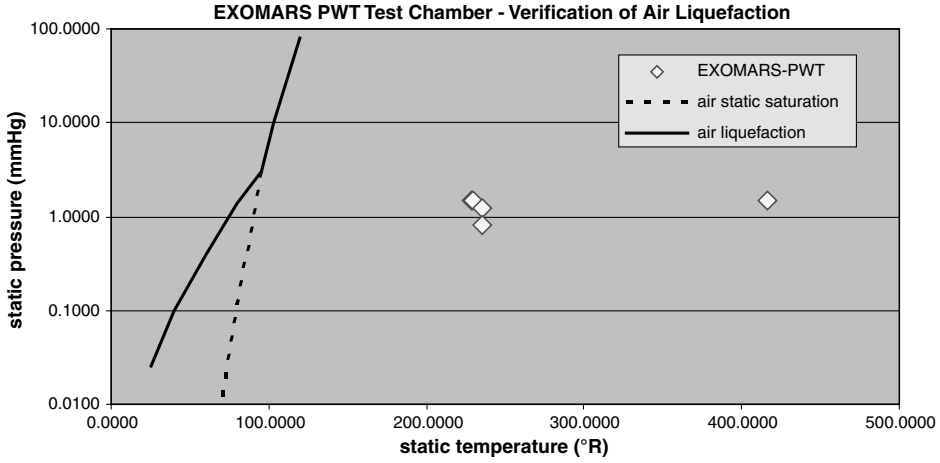

Fig. 23 Verification of air liquefaction in selected EXOMARS-PWT conditions.

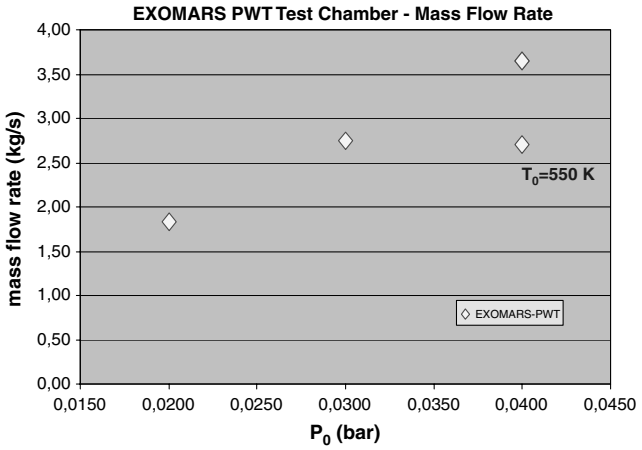

Fig. 24 Mass flow rate requirement.

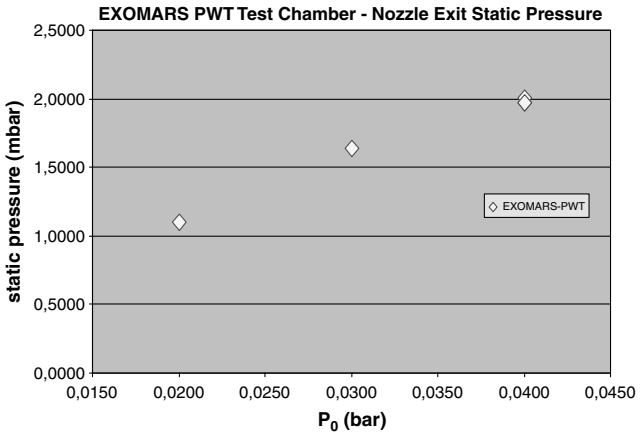

Fig. 25 Test chamber pressure requirement.

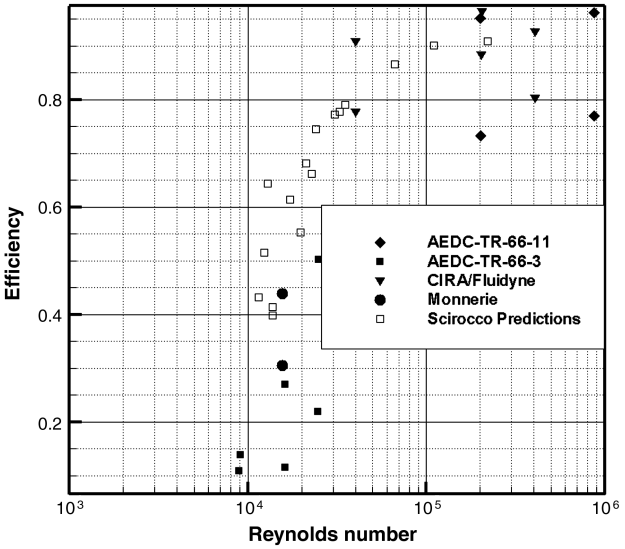

Fig. 26 Diffuser efficiency in function of Reynolds number.

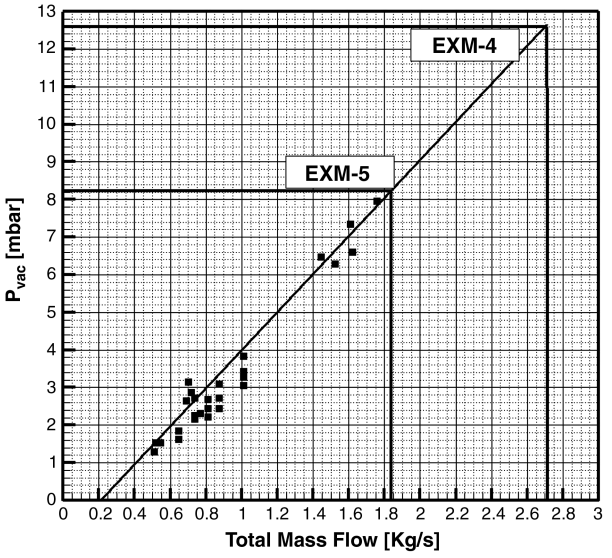

Fig. 27 Vacuum system performance map.

located at $x/D = 10$ from the capsule's base normal wise to the incoming flow, and without porosity effects) for the two nozzle configurations is depicted. Note that in nozzle D configuration the parachute (i.e., the flat plate) is located well inside the diffuser entry, while for nozzle C configuration it is located just at the entry. Both nozzles are interfaced to the new properly designed convergent portion. Moreover, it must be said that for the present axisymmetric simulations no full three-dimensional effects due to test chamber actual geometry have been taken into account.

The goals of these CFD test simulations have been the following: 1) to evaluate the effects of the conical nozzle selection (D is longer, C is shorter) on the overall flowfield; 2) to check the position of the capsule model with respect to the nozzle exit section; 3) to check the position of the parachute model with respect to the diffuser entry section; 4) to evaluate the effects of the interaction between the bow shock wave in front of the capsule and the flow exiting from the nozzle; 5) to evaluate the pressure that establishes inside the test chamber; 6) to evaluate the effects of the capsule wake on the parachute incoming flow; 7) to verify the right functioning of the diffuser, in terms of occurrence of tunnel blockage; and 8) to verify the occurrence of cryogenic temperatures on some facility components (i.e., the available nozzles) that must be absolutely avoided.

The CFD simulations have been conducted in axi-symmetric configuration (nozzle, test chamber with test article inside, diffuser) and both D and C conical nozzles have been considered. The capsule has been positioned 10 cm forward basing an engineering estimation of shock detachment distance [22]. The flow has been modeled axi-symmetric, with no incidence effects, and as ideal gas, fully laminar flow or fully turbulent flow (except for the nozzle flow that is assumed fully laminar), the surfaces have been modeled as cold walls ($T_{\text{wall}} = 300$ K) for nozzle, test chamber and diffuser) or adiabatic

Table 6 Diffuser efficiency estimation

#	P_0 (bar)	T_0 (K)	Re_L	mfr, kg/s	p_{vac}, mbar	Δp_{actual}	Δp_{nsw}	η
EXM-1 (nozzle D)	0.04	300	3.0891E + 05	3.65	14.0	7.09	7.78	0.91
EXM-2 (nozzle D)	0.04	300	3.0891E + 05	3.65	14.0	6.99	7.72	0.91
EXM-3 (nozzle D)	0.04	550	1.4879E + 05	2.71	12.0	6.08	7.78	0.78
EXM-4 (nozzle D)	0.03	300	2.3168E + 05	2.74	12.6	7.46	7.39	1.00
EXM-5 (nozzle D)	0.02	300	1.5445E + 05	1.83	8.2	7.65	7.37	1.04
EXM-4 (nozzle C)	0.03	300	1.0251E + 05	2.74	12.2	3.71	4.97	0.75

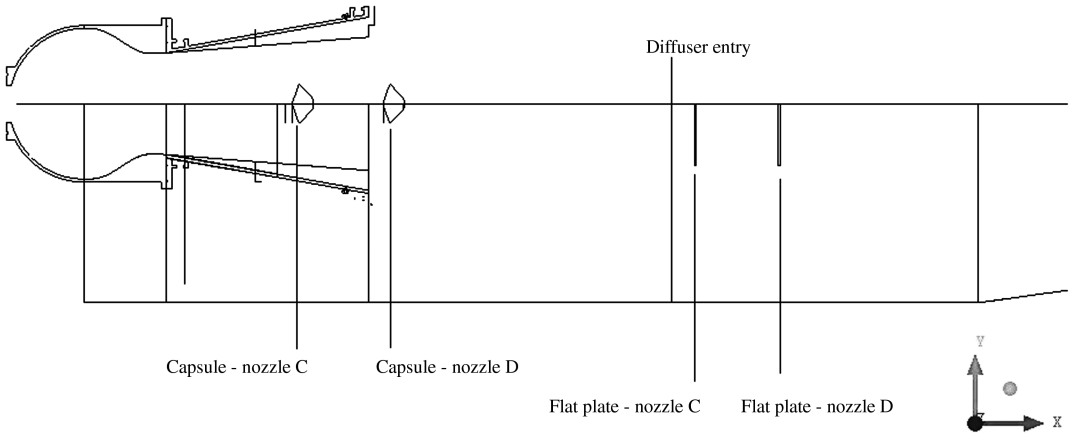

Fig. 28 Test configuration.

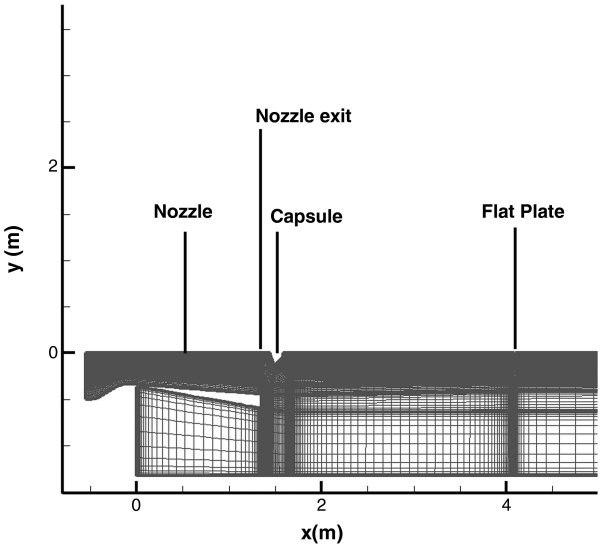

Fig. 29 Test computational grid for nozzle D configuration.

walls (capsule and parachute). The k-ε turbulence modelling by Myong and Kasagi [14] has been used. This model is good enough to describe the boundary layer growing in the turbulent case with respect to the laminar one. This is the main issue of the present turbulent simulations: it is necessary a reliable prediction of boundary layer thickness on the walls of the facility, because a too high value of it could cause the blockage of the wind tunnel. The complex recirculation zones predicted around the parachute are only qualitative, because the parachute geometry is simply modeled as a flat plate, then a more accurate turbulent model will be applied to properly predict its wake when the parachute configuration will be available.

The computational grid shown in Fig. 29, for the facility configuration equipped with the conical nozzle D, is composed by 28 blocks for a total amount of 63,040 cells. The logic of the grid topology is suggested by the general rules reported in paragraph V. In particular, two O-grids have been used around the capsule and the parachute and a shock fitting has been performed. Also in this case, the grid is composed by three grid levels and no differences have been found between the second and the third level in terms of the most sensitive variables (i.e., heat flux and skin friction), thus demonstrating the grid independence of computed results. Note that the present results rely on the finest grid level.

Table 7 reports the test matrix of the four performed CFD simulations: two nozzle configurations in fully laminar and fully turbulent test chamber flow hypothesis.

Figures 30–32 report Mach number contours and streamlines for the facility nozzle D configuration, respectively, showing the flow features in the capsule and parachute region, around the capsule alone and at the diffuser entry and diffuser convergent portion.

A bow shock wave in front of the capsule is predicted (see Figs. 30 and 31), but it does not affect the flow exiting from the nozzle. Note that (see Fig. 31) the expansion originated from the nozzle exit interacts with the bow shock only far from the capsule, thus not affecting the base flow and the wake region of the capsule itself, and therefore the incoming flow to the flat plate simulating the parachute frontal size. The capsule base flow recirculation is predicted to close at about two capsule-lengths downstream of it through a realignment shock, both in laminar and turbulent conditions, so the parachute incoming flow is not disturbed by a reverse flow. Figure 30 shows also a large supersonic region between the capsule and the parachute bounded by the test chamber floor, where large recirculations occur, that, however, do not affect the main stream. A large and unrealistic recirculation bubble is predicted in front of the vertical flat plate that simulates the parachute frontal size, both in laminar and turbulent conditions.

Figure 32 shows the flow features predicted in the diffuser entry region. A strong recirculation bubble backward of the flat plate is predicted in both cases (i.e., laminar and turbulent cases), and the diffuser convergent region is strongly influenced. In the turbulent case the situation is better even though the recirculation closes more forward inside the convergent, because the supersonic region entering the diffuser is larger due to evanishment of the recirculation bubble in the corner of the diffuser floor, predicted in laminar conditions. For the real parachute (i.e., with the actual shape and porosity), the flat plate backward recirculation bubble should be largely reduced or not present, so the flow entering the diffuser is expected supersonic thus allowing for a proper functioning of the subsystem.

In conclusion, it can be said that the analysis of facility nozzle D configuration has verified the feasibility of test, because also simulating the parachute as a vertical flat plate without porosity (no information are still available on the parachute shape and porosity characteristics), that is the worst condition from the fluid dynamic point of view, the main flow entering the diffuser is partially supersonic.

The same flow features have been predicted for nozzle C facility configuration (and then the same flow analysis applies), whose results are shown in Figs. 33–35. The most important difference can be recognized in the predicted position of the recirculation bubble backward of the flat plate reproducing the parachute sizing.

Table 7 Test matrix

Run id.	Configuration	Flow
1	Nozzle D, parachute inside the diffuser entry	Laminar
2	Nozzle D, parachute inside the diffuser entry	Turbulent
3	Nozzle C, parachute at the diffuser entry	Laminar
4	Nozzle C, parachute at the diffuser entry	Turbulent

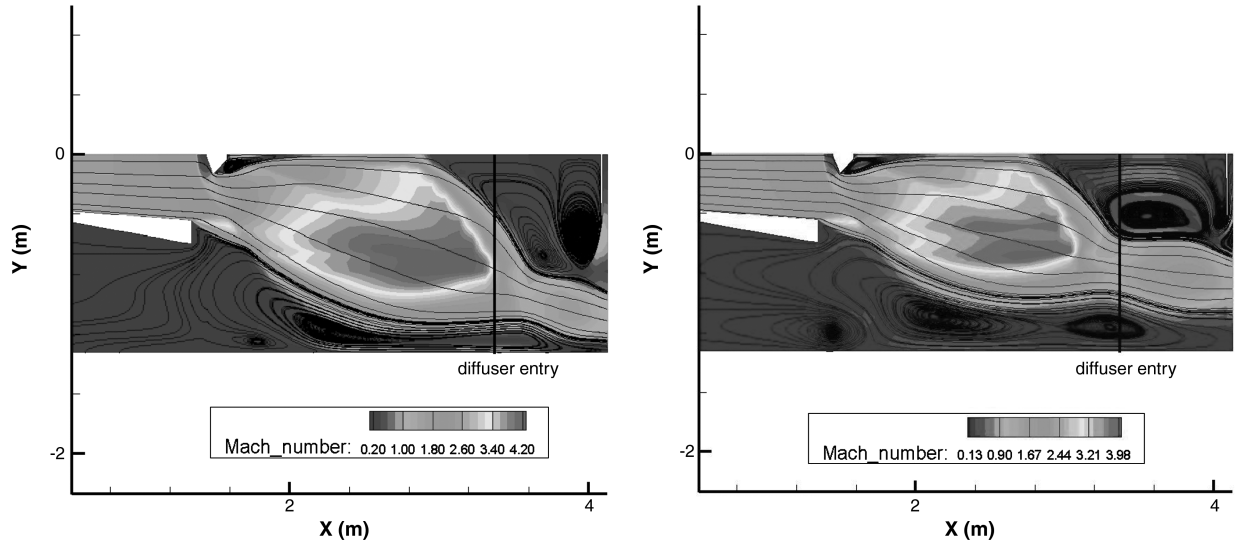

a) Laminar flow b) Turbulent flow

Fig. 30 Nozzle D, Mach number contour map and streamlines (capsule and parachute).

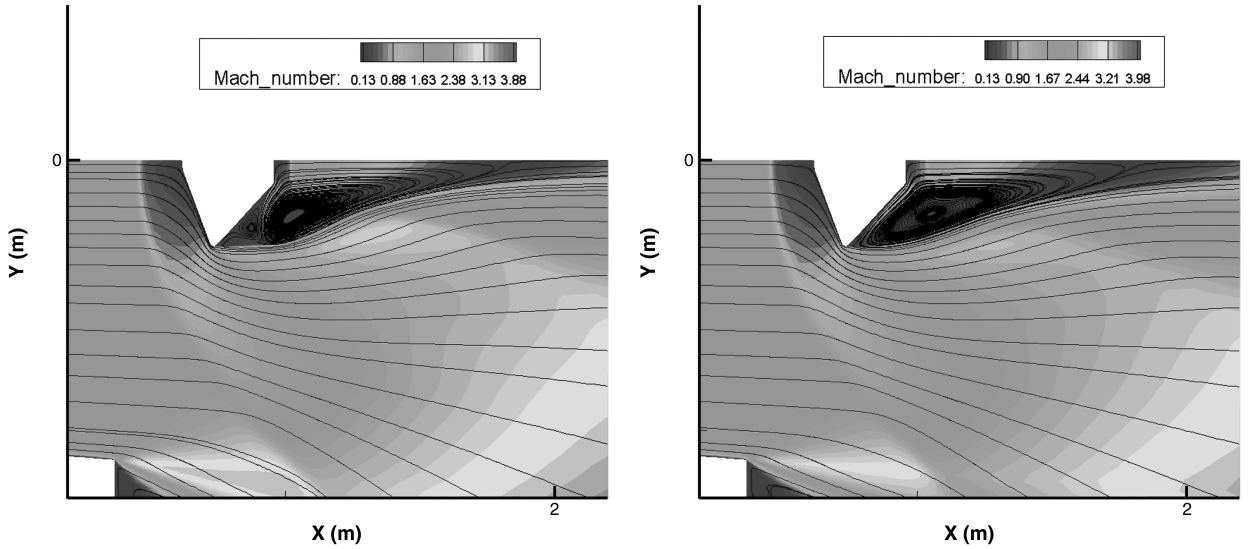

a) Laminar flow b) Turbulent flow

Fig. 31 Nozzle D, Mach number contour map and streamlines (capsule).

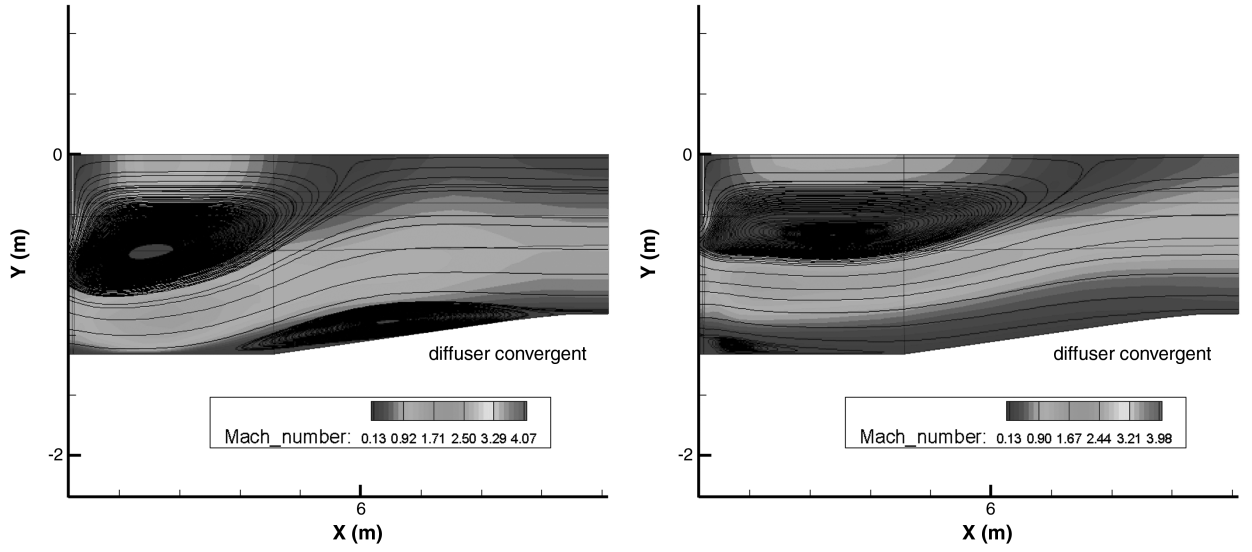

a) Laminar flow b) Turbulent flow

Fig. 32 Nozzle D, Mach number contour map and streamlines (diffuser entry).

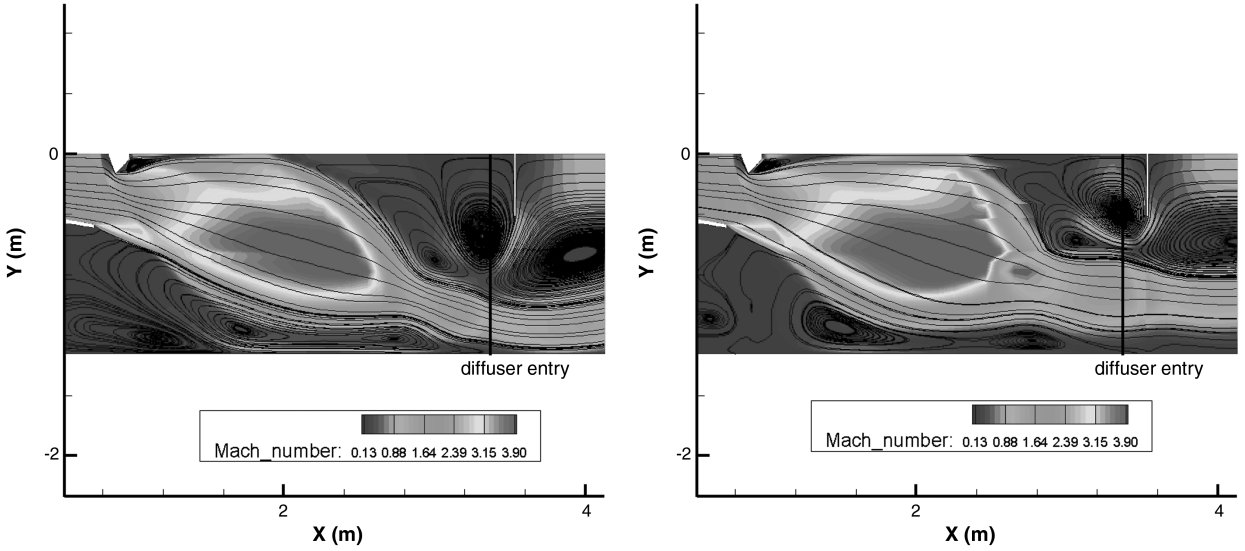

a) Laminar flow b) Turbulent flow

Fig. 33 Nozzle C, Mach number contour map and streamlines (capsule and parachute).

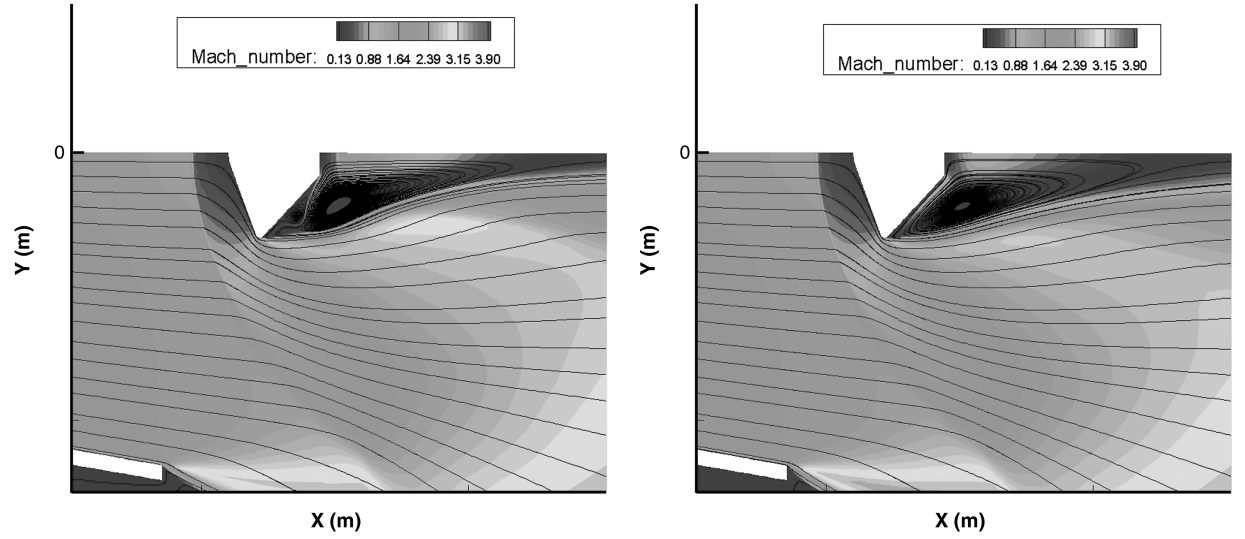

a) Laminar flow b) Turbulent flow

Fig. 34 Nozzle C, Mach number contour map and streamlines (capsule).

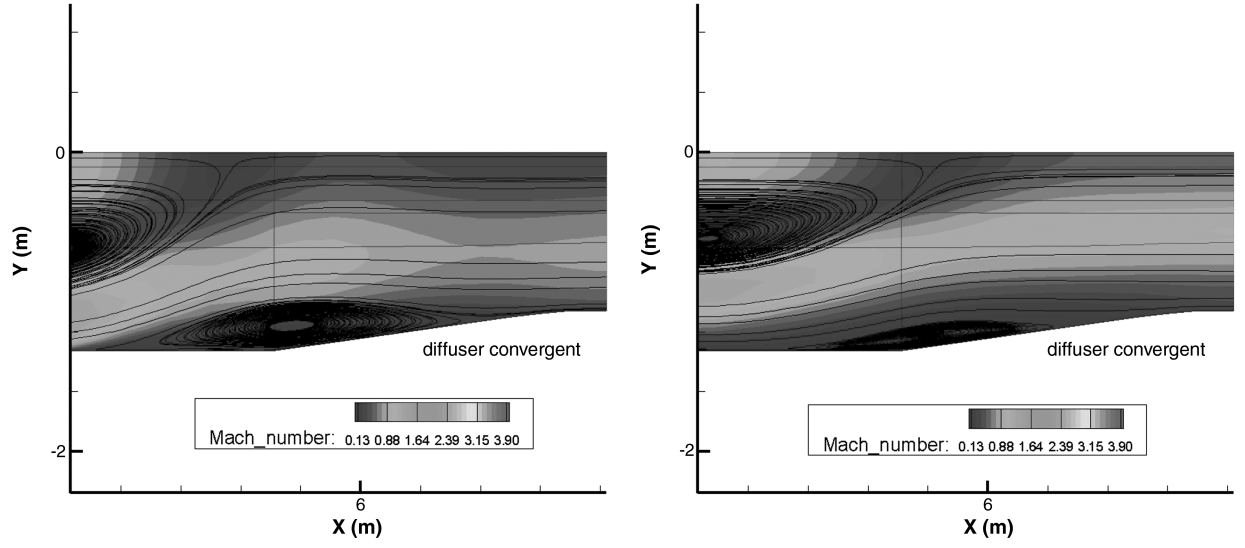

a) Laminar flow b) Turbulent flow

Fig. 35 Nozzle C, Mach number contour map and streamlines (diffuser entry).

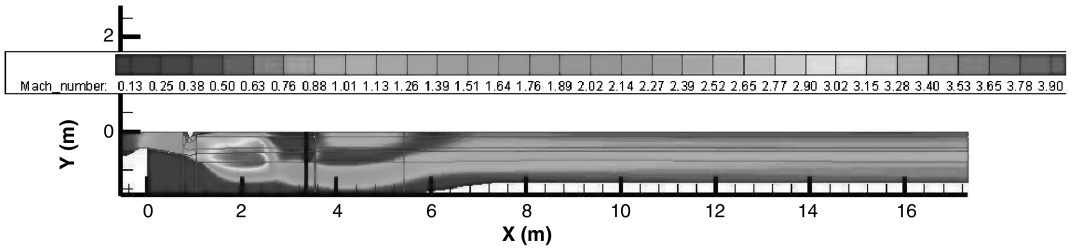

Fig. 36 Nozzle C, Mach number contours (turbulent flow, entire facility).

In fact, the bubble is located more upstream with respect to the diffuser entry (compare Fig. 35 with Fig. 32) as a consequence of the shorter nozzle C configuration, and the influence of this recirculation on the diffuser region is reduced with respect the nozzle D solution. Therefore, a larger portion of the flow entering the diffuser is supersonic, thus inhibiting the risk of blockage (please, keep in mind that we are always working in the worst condition from the fluid dynamic point of view).

The nozzle C configuration of the facility has then resulted the preferred one, following the considerations done on this section, and the entire flowfield in the turbulent case is shown in Fig. 36 in terms of Mach number contour map. It must be also pointed out that no detrimental cryogenic temperature has been predicted on any facility component.

VIII. Conclusions

A feasibility study of ExoMars supersonic parachute experiment to be possibly performed in the CIRA Plasma Wind-Tunnel Scirocco facility has been performed. In particular, the test feasibility analysis has been firstly focused on the capabilities of the facility to match test requirements which simulate the entry in Mars atmosphere. The preliminary wind-tunnel performance evaluation has provided a positive feedback about the possibility to satisfy the test requirements, mainly in terms of test article size, Mach number, and dynamic pressure, provided that a new concept of supersonic nozzle is realized basing on the existing conical nozzle C and a new-design convergent part. The needs in terms of facility subsystems (mass flow rate, vacuum system, mechanical interfaces) have been identified and positively verified, as also the proper functioning of the diffuser in the selected test conditions has been estimated and the presence of cryogenic temperatures has been averted. The possibility to introduce an air heater and/or burner would assure also the matching of temperature requirement, and at the same time would reduce the request of mass flow rate, and could then be considered.

In conclusion, the test has resulted technically feasible in the Scirocco facility with a minimum impact and affordable expected costs.

References

[1] Gily, A., Cassi, C., and Gianfiglio, G., "ExoMars Mission and Spacecraft Architecture," *57th International Astronautical Congress*, International Astronautical Congress Paper 06-A.3.3.05, Oct. 2006.

[2] Lingard, J. et al., "ExoMars Parachute System," *20th AIAA Aerodynamic Decelerator Systems Technology Conference and Seminar*, AIAA Paper 2009-2975, 2009.

[3] Underwood, J. C., "Wind Tunnel Test Plan: WT04," EXM-DM-TP-VOR-00006, Issue 2, Vorticity, Ltd., Jan. 2009.

[4] Lu, F. K., and Marren, D. E., *Advanced Hypersonic Test Facilities*, Progress in Astronautics and Aeronautics, Vol. 198, AIAA, Reston, VA, 2002, Ch. 11.

[5] De Filippis, F., Caristia, S., Del Vecchio, A., and Purpura, C., "The Scirocco PWT Facility Calibration Activities," *3rd International Symposium Atmospheric Reentry Vehicle and Systems*, AAAF, Arcachon, France, March 2003.

[6] Mitcheltree, R., "High Altitude Test Program For A Mars Subsonic Parachute," *18th AIAA Aerodynamic Decelerator Systems Technology Conference and Seminar*, AIAA Paper 2005-1659, 2005.

[7] Sengupta, A., Kelsch, R., Roeder, J., Wernet, M., Witkowski, A., and Kandis, M., "Supersonic Performance of Disk-Gap-Band Parachutes Constrained to a 0-Degree Trim Angle," *Journal of Spacecraft and Rockets*, Vol. 46, No. 6, Nov.–Dec. 2009, pp. 1155–1163. doi:10.2514/1.41223

[8] Haya-Ramos, R. et al., "ExoMars Mission Analysis and Design from Mars Arrival to Landing," *6th International Planetary Probe Workshop*, Georgia Inst. of Technology, Atlanta, GA, 2008.

[9] Marini, M. et al., "Test Design Methodologies for Flight Relevant Plasma Wind Tunnel Experiments," *Invited Lecture, West-East High Speed Flow Field Conference*, Moscow, Russia, 2007.

[10] Park, C., "A Review of Reaction Rates in High Temperature Air," AIAA Paper 89-1740, June 1989.

[11] Millikan, R. C., and White, D. R., "Systematic of Vibrational Relaxation," *The Journal of Chemical Physics*, Vol. 39, No. 12, 1963, pp. 3209–3213. doi:10.1063/1.1734182

[12] Park, C., and Lee, S. H., "Validation of Multi-Temperature Nozzle Flow Code NOZNT," AIAA Paper 93-2862, 1993.

[13] Yun, K. S., and Mason, E. A., "Collision Integrals for the Transport Properties of Dissociating Air at High Temperatures," *Physics of Fluids*, Vol. 39, No. 12, 1962, pp. 3209–3213.

[14] Myong, H. K., and Kasagi, N., "A New Approach to the Improvement of *k-e* Turbulence Model for Wall-Bounded Shear Flows," *JSME International Journal*, Vol. 33, 1990, pp. 63–72.

[15] Grasso F., and Falconi, D., "High-Speed Turbulence Modeling of Shock-Wave/Boundary-Layer Interaction," *AIAA Journal*, Vol. 31, No. 7, July 1993, pp. 1199–1206.

[16] Borrelli, S., and Pandolfi, M., "An Upwind Formulation for the Numerical Prediction of Non Equilibrium Hypersonic Flows," *12th International Conference on Numerical Methods in Fluid Dynamics*, Oxford Univ., Oxford, England, 1990.

[17] Pope, A., and Goin, K. L., *High Speed Wind Tunnel Testing*, Krieger Publishing Company, Malabar, FL, 1965.

[18] Risch, T. K., "Process Integrator Services PWT Plasma Diffuser Performance Specification Verification," Aerotherem Corporation Document No. SCI-VP-10000D-0016-AETH.

[19] Monnerie, B., "Etude d'une famille de diffuseurs pour soufflerie hypersonique a faible nombre de Reynolds," *La Recherche Aerospatiale: Bulletin Bimestriel de l'Office National d'Etudes et de Recherches Aerospatiales*, Vol. 114, Sept.–Oct. 1966, pp. 9–16.

[20] Ferrigno, F., "Efficienza del Diffusore di una Galleria Ipersonica a Bassi Numeri di Reynolds," *Proceedings of XIV AIDAA National Congress*, AIDAA, Naples, Italy, Oct. 1997, pp. 163–172.

[21] Risch, T. K., "Process Integrator Services PWT Vacuum System Performance Specification Verification," Aerotherem Corporation SCI-VP-10000D-0028-AETH.

[22] Anderson, J. D., Jr., *Hypersonic and High Temperature Gas Dynamics*, McGraw–Hill, New York, 1989.

R. Cummings
Associate Editor